DOI: https://doi.org/10.15625/0868-3166/22195

# Debye-Waller factor of Pt in X-ray absorption fine structure analyzed using classical anharmonic correlated Einstein model

Nguyen Huy Thao<sup>1</sup>, Nguyen Thi Minh Thuy<sup>2</sup>, Dang Sy Lan<sup>2</sup>, Le Viet Hoang<sup>3</sup> and Tong Sy Tien<sup>2,†</sup>

E-mail: †tongsytien@yahoo.com

Received 8 January 2025 Accepted for publication 28 July 2025 Published 25 September 2025

**Abstract.** An investigation of the Debye-Waller (DW) factor associated with the anharmonic extended X-ray absorption fine structure (XAFS) of crystalline platinum (Pt) has been carried out, taking into account the effects of the thermal disorder. The DW factor was derived in explicit and analytically tractable expressions based on a theoretical framework that incorporates an anharmonic effective potential and employs classical statistical theory within the correlated Debye model. Thermodynamic parameters of Pt were evaluated by considering the influence of nearestneighbor atoms on both the absorber and the backscatterer. The numerical results for Pt over the temperature range of 0–800 K show excellent agreement with experimental data and alternative theoretical approaches. These findings confirm the capability of the present model to effectively describe and analyze the anharmonic behavior of the XAFS Debye-Waller factor for similar metals, particularly those exhibiting complex thermal dynamics.

Keywords: XAFS Debye-Waller factor; Einstein model, thermal disorder; crystalline platinum. Classification numbers: 61.05.cj; 63.20.Ry; 65.40.De.

### 1. Introduction

Nowadays, many structural parameters and thermodynamic properties of materials can be identified using the X-ray absorption fine structure (XAFS) data analysis [1]. For a given scattering

<sup>&</sup>lt;sup>1</sup>Department of Physics, Hanoi Pedagogical University 2, Vinh Phuc 283460, Vietnam

<sup>&</sup>lt;sup>2</sup>Faculty of Fundamental Sciences, University of Fire Prevention and Fighting, Hanoi 120602, Vietnam

<sup>&</sup>lt;sup>3</sup>Department of Physics, Hanoi University of Science, Hanoi 120034, Vietnam

path, the *K*-edge XAFS signal is expressed in distance-dependent factors of a canonical average, which includes a non-Gaussian disorder in the form [2]:

$$\chi(k,T) = \frac{Ne^{-2k^2\sigma^2(T)}f(k)}{kR^2(T)}\sin\left[2kR(T) + \delta(k)\right],\tag{1}$$

where N is the neighboring atomic number, k is the wavenumber of the photoelectron, T is the absolute temperature, f(k) and  $\delta(k)$  are characteristic parameters for photoelectron scattering,  $\sigma^2(T)$  is the mean-square relative (MSR) displacement or the  $2^{\text{nd}}$ -XAFS cumulant, and R(T) is the distance between neighboring atoms.

However, thermal disorders are sensitive to XAFS oscillations and cause anharmonic effects [3], as seen in Fig. 1, so their influence should be considered in the XAFS signal analysis.

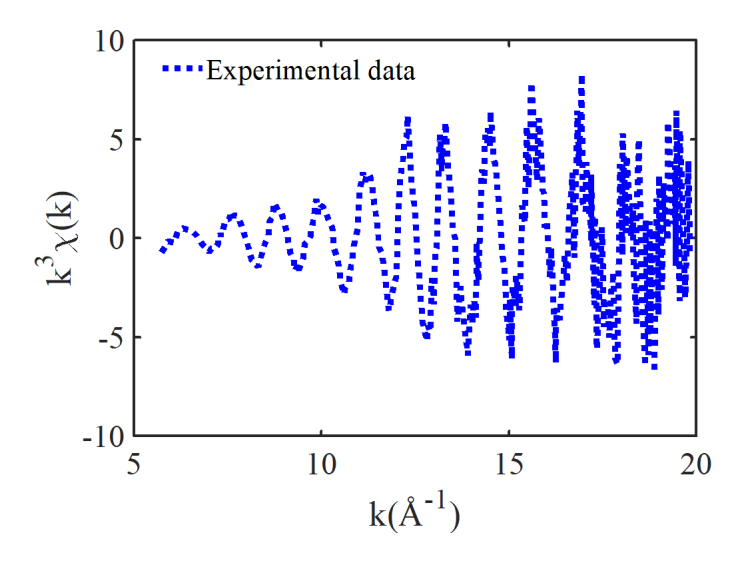


**Fig. 1.** The K-edge XAFS signal  $k^3\chi(k)$  of Pt foil is obtained from the experimental data [4].

The Debye-Waller (DW) factor [5] is important in investigating the anharmonic XAFS signal because it describes the XAFS amplitude reduction and thermal disorder in terms of temperature and wavenumber dependencies. It is usually defined in the following form [6]:

$$W(T,k) = \exp\{-2k^2\sigma^2(T)\}.$$
 (2)

Currently, platinum (Pt) possesses physical and chemical characteristics that ensure stability [7], which enables its use in jewelry, chemical catalysts, magnetic disks, and sensors, as well as in various electronic, automotive, medical, and other industries [8]. Beyond these practical applications, Pt is widely recognized as a model system for studying vibrational dynamics and thermal disorder in solids, particularly through XAFS spectroscopy [4], owing to its status as a heavy element with pronounced anharmonic behavior and a well-characterized phonon spectrum [7, 8]. Meanwhile, the experimental XAFS cumulants of Pt at temperatures from 200 to 800 K were measured by Okube and Yoshiasa at beamline BL10B of Photon Factory in the National Laboratory for High Energy Physics (KEK-PF, Tsukuba, Japan) [9]. The anharmonic correlated Debye (ACD) model has also been applied by Duc *et al.* to calculate the second cumulant of Pt [10].

Still, the derived thermodynamic parameters remain cumbersome to use due to the complexity of the temperature-dependent expressions obtained from the experimental XAFS data.

Recently, the classical anharmonic correlated Einstein (CACE) model has emerged as a convenient theoretical approach for analyzing anharmonic XAFS data. It offers the advantage of yielding simple and explicit expressions for anharmonic XAFS parameters [11], enabling efficient analysis of metallic systems [12]. Although previous studies have employed the modified CACE models to calculate anharmonic XAFS parameters of certain metals within the DF formalism, it has not yet been applied to analyze the anharmonic DW factor under thermal disorder systematically. Therefore, applying the CACE model to the anharmonic XAFS DW factor analysis of Pt is crucial for enhancing the interpretation of experimental XAFS data.

# 2. Theoretical calculation model

In the framework of anharmonic XAFS theory, the MSR displacement is fundamentally linked to the low-order moments of the true radial pair distribution (RP) function. This displacement can be quantitatively described by the following expression [13]:

$$\sigma^{2} = \left\langle (r - \langle r \rangle)^{2} \right\rangle = \left\langle (x - \langle x \rangle)^{2} \right\rangle = \left\langle x^{2} \right\rangle - \left\langle x \right\rangle^{2}, \tag{3}$$

where the angular brackets  $\langle \rangle$  denote the thermal average, and  $x = r - r_0$  represents the deviation of the instantaneous bond length from its equilibrium value. Here, r and  $r_0$  correspond to the instantaneous and equilibrium distances between the absorbing and backscattering atoms, respectively.

Normally, determining the anharmonic effective (AE) potential of a system is necessary to identify its thermodynamic parameters [14]. The AE potential in the relative vibrations of backscattering (B) and absorbing (A) atoms can be calculated using the pair interaction (PI) potential [15]:

$$V_{eff} = \varphi(x) + \sum_{i=A,B} \sum_{j \neq A,B} \varphi\left(\varepsilon_{i} x \hat{R}_{AB} \hat{R}_{ij}\right), \ \varepsilon_{i} = \frac{\mu}{M_{i}}, \tag{4}$$

where  $\hat{R}$  is the bond unit vector, sum i is the over-absorbing and backscattering atoms, the sum j is over all their nearest neighbors,  $\mu = M_A M_B / (M_A + M_B)$  is the reduced mass of a single bond pair with atomic masses  $M_A$  and  $M_B$ ,  $\varphi(x)$  is a PI potential of these atoms,  $\varphi\left(\varepsilon_i x \hat{R}_{AB} \hat{R}_{ij}\right)$  is the nearest-neighbor atomic contributions and characterizes the correlation effect caused by these atoms on the PI potential.

The crystalline structure of Pt is represented in Fig. 2, comprising identical atoms arranged such that eight atoms occupy the cube corners and six atoms are centered on each face [16]. This arrangement corresponds to a face-centered cubic (FCC) lattice in which each unit cell contains four atoms [17]. Based on these structural characteristics, the AE potential for Pt is evaluated by Eq. (4) and is expressed as follows:

$$V_{eff}(x) = \varphi(x) + 4\varphi(0) + 2\varphi\left(-\frac{x}{2}\right) + 8\varphi\left(\frac{x}{4}\right) + 8\varphi\left(-\frac{x}{4}\right). \tag{5}$$

Usually, the AE potential of metals can be validly determined from the Morse potential [18], which can be expanded up to the 4th order around its minimum position:

$$\varphi(x) = D\left(e^{-2\alpha x} - 2e^{-\alpha x}\right) \cong -D + D\alpha^2 x^2 - D\alpha^3 x^3 + 7D\alpha^4 x^4 / 12,$$
 (6)

where D is the dissociative energy and  $\alpha$  characterizes the potential width.

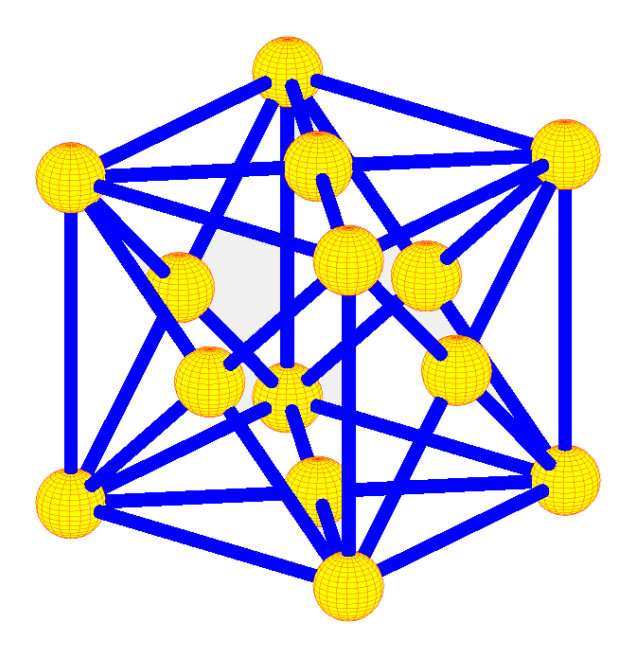


Fig. 2. The atomic structure of Pt.

Utilizing this PI potential to calculate the AE potential by Eq. (5). The obtained result is presented by ignoring constant terms as follows:

$$V_{eff}(x) = \frac{1}{2}k_{eff}x^2 - k_{an3}x^3 + k_{an4}x^4,$$
(7)

where  $k_{eff}$  is the effective force constant, and  $k_{an3}$  and  $k_{an4}$  are the anharmonic force constants. These constants are expressed in a temperature-independent form as follows:

$$k_{eff} = 5D\alpha^2, \quad k_{an3} = 5D\alpha^3/4, \quad k_{an4} = 133D\alpha^4/192.$$
 (8)

The CACE model is formulated from the correlated Einstein model [19], incorporating the AE potential [15] within the framework of classical statistical theory [20]. In the crystal lattice, atomic thermal vibrations are regarded as phonons and described through the correlated Einstein temperature  $\theta_E$  and frequency  $\omega_E$  [11]. The effective force constant is employed to determine these parameters for Pt, as expressed below:

$$\omega_E = \sqrt{\frac{k_{eff}}{\mu}} = \alpha \sqrt{\frac{10D}{m}}, \ \theta_E = \frac{\hbar \omega_E}{k_B} = \frac{\hbar \alpha}{k_B} \sqrt{\frac{10D}{m}},$$
 (9)

where and  $\hbar$  and  $k_B$  are the reduced Planck and Boltzmann constants, respectively.

In the classical-statistical limit, the moments  $\langle x^k \rangle$  were determined by Stern *et al.* based on evaluating the thermal average [20]:

$$\left\langle x^{k} \right\rangle = \frac{\int_{-\infty}^{\infty} x^{k} \exp\left[-\frac{V_{eff}(x)}{k_{B}T}\right] dx}{\int_{-\infty}^{\infty} \exp\left[-\frac{V_{eff}(x)}{k_{B}T}\right] dx}.$$
 (10)

Utilizing the AE potential in Eq. (7) and expanding approximately to  $3^{rd}$ -order, which is written as

$$\left\langle x^{k} \right\rangle \approx \frac{\int_{-\infty}^{\infty} x^{k} \exp\left[\frac{-k_{eff}x^{2}}{2k_{B}T}\right] \left[\sum_{n=0}^{3} \frac{1}{n!} \left(\frac{k_{an3}x^{3} - k_{an4}x^{4}}{k_{B}T}\right)^{k}\right] dx}{\int_{-\infty}^{\infty} \exp\left[\frac{-k_{eff}x^{2}}{2k_{B}T}\right] \left[\sum_{n=0}^{3} \frac{1}{n!} \left(\frac{k_{an3}x^{3} - k_{an4}x^{4}}{k_{B}T}\right)^{k}\right] dx}.$$
(11)

The temperature-dependent general expression of the MSR displacement in the CACE model can be obtained by Eqs. (3) and (10) with the lowest order in *T* is:

$$\sigma^{(2)} = \frac{k_B T}{k_{\text{eff}}} \left[ 1 - \frac{12k_B T}{k_{eff}^2} \left( k_4 - \frac{3k_3^2}{k_{eff}} \right) \right] \approx \frac{k_B T}{k_{\text{eff}}}.$$
 (12)

After replacing the expressions of local force constants  $k_{eff}$ ,  $k_{an3}$ , and  $k_{an4}$  in Eq. (8) into this general expression, we obtain the temperature-dependent MSR displacement of Pt in the following form:

$$\sigma^{2}(T) = \frac{k_{B}T}{5D\alpha^{2}} \left( 1 + \frac{47k_{B}T}{400D} \right) \approx \frac{k_{B}T}{5D\alpha^{2}}.$$
 (13)

Substituting this obtained MSR displacement into Eq. (2), the temperature-dependent XAFS DW factor of Pt is written as

$$W(T,k) = \exp\left\{-\frac{2k_B}{5D\alpha^2}k^2T\right\}. \tag{14}$$

Thus, the anharmonic XAFS DF factor of Pt has been effectively evaluated under the influence of thermal disorder through the extension of the CACE model. The analytical expression obtained from this extended CACE model successfully captures essential physical properties expected in the temperature-dependent regime, ensuring consistency with the thermodynamic behavior of the system.

# 3. Results and discussions

In this section, The expressions developed in Sec. 2 are utilized to perform numerical calculations for Pt based on its intrinsic physical parameters. Herein, the atomic mass of m = 195.084u is identified by Mermin & Ashcroft [17], and the Morse potential parameters of Pt are  $r_0 = 2.7622\text{Å}$ ,  $\alpha = 1.3412\text{Å}^{-1}$ , and D = 0.5896eV identified from the experimental XAFS data [9] using an effective method for metals proposed by Pirog *et al.* [21].

The values of the local force constants  $k_{eff}$ ,  $k_{an3}$ ,  $k_{an4}$  along with the correlated Einstein frequency  $\omega_E$  and temperature  $\omega_E$  of Pt, are determined from Eqs. (8)–(9) and summarized in Table 1. These results are calculated using the present CACE model with the previously introduced Morse potential parameters. For comparison, the experimental data reported by Nedoseikina and Pirog [22] were obtained at the Synchrotron Radiation Siberian Center (SRSC, Siberia, Russia), where the correlated Einstein frequency and temperature were extracted based on the effective force constant. In contrast, the values derived from the ACD model are calculated using the correlated Debye temperature and frequency, employing the tight-binding 2<sup>nd</sup>-moment approximation (TB-SMA) potential [10]. Notably, our calculated results show excellent agreement with both the ACD model [10] and the experimental data [22], particularly in terms of the correlated Einstein frequency and temperature.

**Table 1.** The physical parameters of Pt and its thermodynamic parameters are obtained from the experimental data and the present CACE and ACD models.

Method	$(eV \mathring{A}^{-2})$	$(eV \mathring{A}^{-3})$	$(eV \mathring{A}^{-4})$	$(10^{13} \text{Hz})$	(K)
CACE model	5.30	1.78	1.32	2.29	175
ACD model	5.26	2.79	_	2.28	174
Experimental data	$5.0\pm0.2$	$2.0\pm0.1$	_	$2.22\pm0.05$	$170 \pm 4$

<sup>&</sup>lt;sup>a</sup> Our values are obtained using the present CACE model.

<sup>&</sup>lt;sup>c</sup> The values are obtained from the experimental data measured by Nedoseikina & Pirog [22].

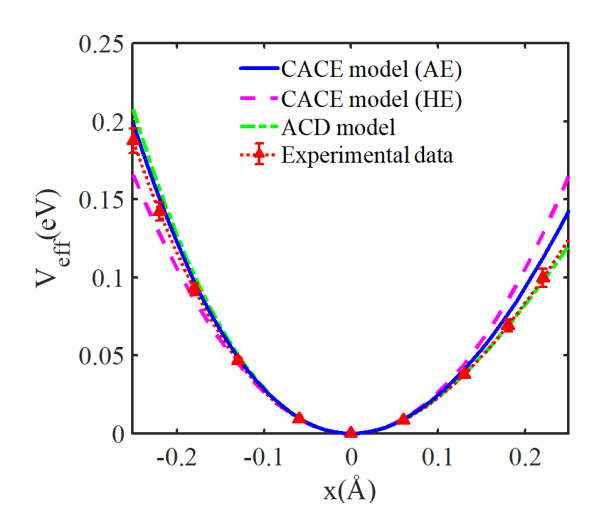


**Fig. 3.** The position-dependent HE and AE potentials of Pt are obtained from the present CACE and ACD [10] models and experimental data [22].

The harmonic effective (HE) and AE potentials of Pt within the position range from -0.25 to 0.25 Åare depicted in Fig. 3. The result obtained from the present CACE model is calculated by Eqs. (7) and (8), whereas the results from the ACD model [10] and experimental data [22] are calculated by Eq. (7) in the expansion to the  $3^{rd}$ -order with the local force constants listed in Table 1. Herein, the HE potential only considers the first term, and the AE potential considers all terms in Eq. (7). It is evident that our result shows good agreement with both the ACD model [10] and experimental data [22], particularly in the vicinity of the equilibrium position (x = 0). Moreover, the further away from the equilibrium position, the AE potential is influenced more strongly by the anharmonic effect caused by terms ( $-k_{an3}x^3$ ) and ( $k_{an4}x^4$ ), especially for the contribution of the term ( $k_{an4}x^4$ ) that is considered in the present CACE model, as seen in Fig. 3.

The MSR displacement  $\sigma^2(T)$  of Pt at temperatures from 0 to 800 K is illustrated in Fig. 4. Our obtained result from the present CACE model is calculated by Eq. (13), and the obtained result from the ACD model is calculated by Duc *et al.* [10]. Meanwhile, experimental XAFS results at 200 K, 300 K, 400 K, 600 K, and 800 K were measured by Okube & Yoshiasa at the BL10B of KEK-PF, Tsukuba, Japan [9]. It is observable that our results fit with those obtained

<sup>&</sup>lt;sup>b</sup> The values are obtained from the ACD model reported by Duc et al. [10].

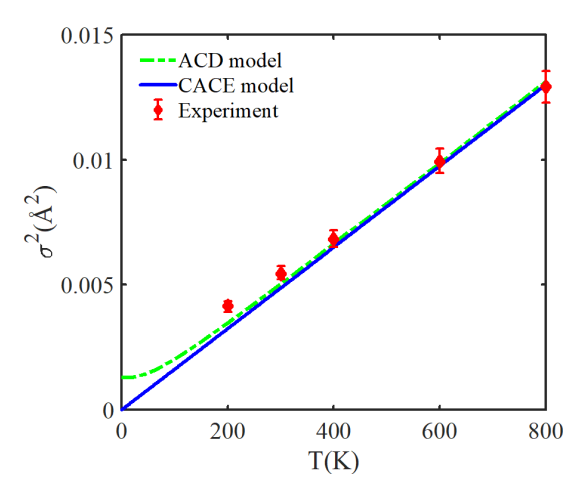


**Fig. 4.** The temperature-dependent MSR displacement of Pt is obtained from the experiment [9] and the present CACE and ACD [10] models.

from the experiment [9] and the ACD model (for temperatures are not too low) [10]. Herein, the CACE model adopts a single effective frequency to represent thermal vibrations in the crystal lattice. Although this approach does not account for the acoustic phonon branch, it provides a significant advantage in terms of computational simplicity and efficiency, making it highly suitable for practical applications. In contrast, the ACD model considers phonon dispersion by employing variable frequencies, allowing for a more detailed description of the acoustic phonon branch, but at the cost of increased computational complexity. Therefore, each calculation model offers distinct advantages and limitations in the analysis of anharmonic XAFS data, as seen in Fig. 4.

**Table 2.** The MSR displacements of Pt obtained from experiment and the present CACE and ACD models.

T (K)	$(\mathring{\text{A}}^2)^a$	$(\mathring{\text{A}}^2)^b$	$(\mathring{\text{A}}^2)^c$	$(\mathring{\text{A}}^2)^d$
200	0.32	0.35	0.42	0.24
300	0.48	0.51	0.54	0.30
400	0.64	0.67	0.68	0.36
600	0.96	0.99	0.99	0.52
800	1.29	1.33	1.29	0.64

<sup>&</sup>lt;sup>a</sup> Our values obtained using the present CACE model.

The values of the MSR displacement of Pt at several temperatures are given in Table 2. It is observable that although the result obtained from the present CACE model reaches zero as the temperature approaches zero, it still works well in the temperature region. The reason is that the present CACE model only employs classical statistical theory and cannot calculate quantum effects, unlike the ACD model [10]. Still, the contribution of this effect is only significant at low

<sup>&</sup>lt;sup>b</sup> Values from the ACD model reported by Duc et al. [10].

<sup>&</sup>lt;sup>d</sup> Experimental values measured by Okube & Yoshiasa [9].

temperatures, so there is no influence on the obtained results in the high-temperature region, even at room temperature.

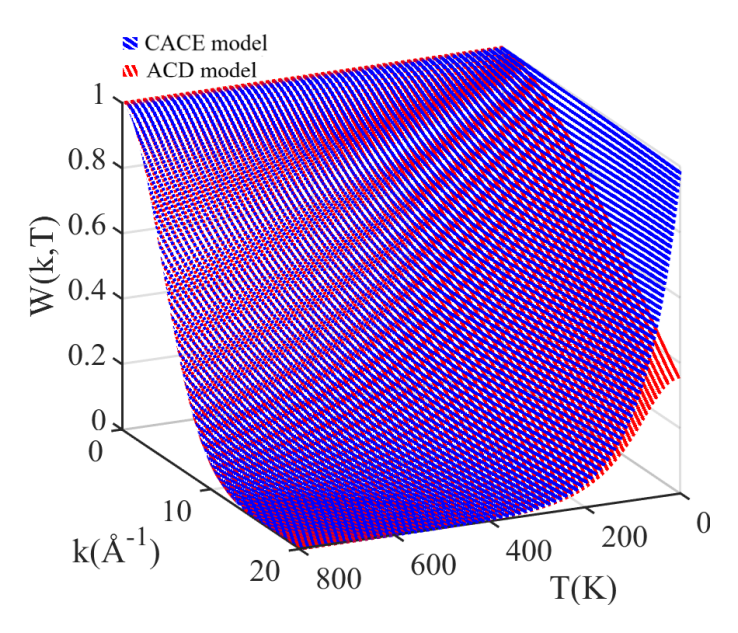


**Fig. 5.** The temperature and wavenumber dependencies of the XAFS DW factor of Pt are obtained from the present CACE and ACD [10] model.

The anharmonic XAFS DW factor W(T,k) of Pt as a function of temperature (0–800 K) and wavenumber (0–20 Å $^{-1}$ ) is presented in Fig. 5. The results obtained from the present CACE model are calculated by Eq. (14), whereas those from the ACD model are derived from Eq. (2), with the temperature-dependent MSR displacement taken from Ref. [10]. It is observed that the anharmonic XAFS DW factor behaves as an inverse function with respect to both temperature T and wavenumber k. Furthermore, a good agreement is found between our results and those obtained from the ACD model [10] in the temperature range  $T \ge \theta_E$ , as seen in Fig. 5.

The logarithm of XAFS DW factor  $\ln[W(T,k)]$  of Pt at 400 K, 600 K, and 800 K and wavenumbers from 0 to 20 Åis illustrated in Fig. 6. Herein, our obtained results from the present CACE model are calculated by Eq. (14), and the experimental results with error bars are obtained by Eq. (2) using the measured MSR displacement data [9]. Meanwhile, the result from the ACD model is calculated by Eq. (2), with the MSR displacement values taken from Ref. [10]. It is evident that our results exhibit good agreement with both the experimental data [9] and the ACD model [10], particularly at higher wavenumbers and elevated temperatures, as seen in Fig. 6.

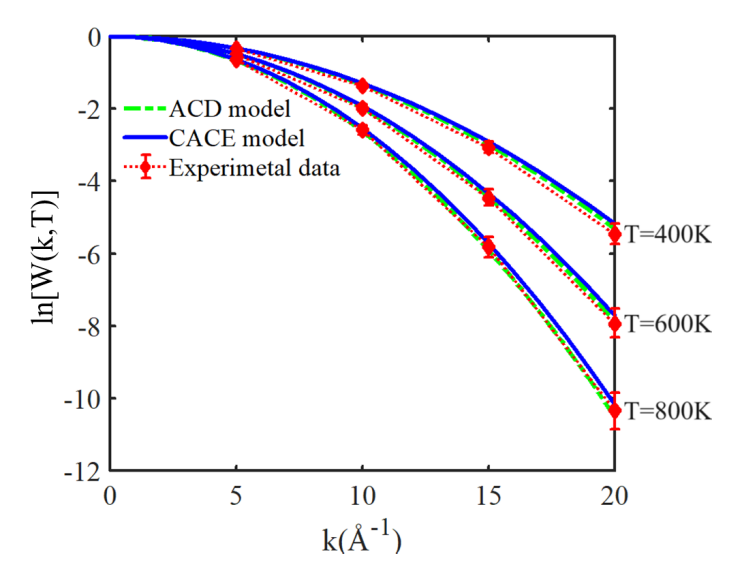


**Fig. 6.** The wavenumber-dependent logarithms of the XAFS DW factor of Pt in the temperature change are obtained from the experimental data [9] and the present CACE and ACD [10] models.

Table 3: The logarithms of the XAFS DW factor of Pt are obtained from the experimental data and the present CACE and ACD models at various wavenumbers and temperatures.

<i>T</i> (K)	k (Å <sup>-1</sup> )	CACE model <sup>a</sup>	ACD model <sup>b</sup>	Experimental data <sup>e</sup>
400	5	-0.32	-0.33	-0.34±0.02
600	5	-0.48	-0.49	$-0.50\pm0.03$
800	5	-0.64	-0.66	$-0.65 \pm 0.04$
400	10	-1.30	-1.33	$-1.37 \pm 0.07$
600	10	-1.93	-1.97	$-1.99\pm0.10$
800	10	-2.54	-2.63	$-2.58\pm0.13$
400	15	-2.92	-2.99	$-3.07 \pm 0.16$
600	15	-4.33	-4.44	$-4.47 \pm 0.22$
800	15	-5.72	-5.91	$-5.81 \pm 0.28$
400	20	-5.18	-5.32	$-5.46 \pm 0.28$
600	20	-7.71	-7.89	$-7.94 \pm 0.40$
800	20	-10.18	-10.51	$-10.34 \pm 0.49$

<sup>&</sup>lt;sup>a</sup> Our values are obtained using the present CACE model.

<sup>&</sup>lt;sup>b</sup> The values are obtained from the ACD model reported by Duc et al. [10].

<sup>&</sup>lt;sup>e</sup> The values are obtained from the experimental data measured by Okube & Yoshiasa [9].

The calculated values of the logarithm of the XAFS DW factor of Pt at various wavenumbers and temperatures are listed in Table 3. It can be observed that the logarithmic values decrease significantly with increasing temperature T and wavenumber k. This behavior arises from the fact that the logarithm of the XAFS DW factor is linearly dependent on T and quadratically dependent on T and quadratically dependent on T and experimental data [9], the present results demonstrate improved accuracy at elevated temperatures. This improvement stems from the enhanced capability of the CACE model to accurately capture the anharmonic effects induced by thermal disorder in the crystal lattice. Hence, this model enables the direct extraction of key physical parameters from experimental EXAFS data in a simple way at not-too-low temperatures (even below room temperature for most metals).

#### 4. Conclusion

In this study, we have developed an appropriate calculation model to investigate the anharmonic XAFS DW factor of Pt under the influence of thermal disorder. The expressions derived from the present CACE model satisfy fundamental requirements in the temperature-dependent regime. As the temperature T increases and the wavenumber k becomes larger, the anharmonic XAFS DW factor decreases accordingly. Consequently, the anharmonic XAFS amplitude exhibits a more pronounced reduction at higher temperatures and larger wavenumbers. The reason is that the anharmonic XAFS amplitude is proportional to the anharmonic XAFS DW factor. This thermodynamic property indicates that the anharmonic effects at higher temperatures more rapidly influence the XAFS signal of Pt.

Our numerical results for Pt show good agreement with those obtained from the ACD model and experimental data across a wide range of temperatures. This consistency confirms the effectiveness of the present CACE model in analyzing the anharmonic XAFS DW factor of Pt. Moreover, this model can be extended to investigate the anharmonic XAFS DW factors of other FCC metals within the temperature range from above the correlated Einstein temperature up to just below the melting point, particularly those exhibiting complex thermal dynamics.

# Acknowledgments

This research is funded by the Vietnam National Foundation for Science and Technology Development (NAFOSTED) under grant number 103.01-2023.32.

# **Conflict of interest**

The authors have no conflict of interest to declare.

#### References

- [1] J. J. Rehr, J. J. Kas and F. D. Vila, *X-ray absorption spectroscopy and related techniques*, International Tables for Crystallography I (2024) 71.
- [2] M. Newville, Fundamentals of xafs, Rev. Mineral. Geochem. 78 (2014) 33.
- [3] R. B. Greegor and F. W. Lytle, Extended x-ray absorption fine structure (exafs) study of ni alloys, Phys. Rev. B 20 (1979) 4902.
- [4] Y. Nishihata, O. Kamishima, Y. Kubozono, H. Maedab and S. Emura, *Xafs studies using a position-sensitive silicon microstrip detector*, J. Synchrotron Radiat. **5** (1998) 1007.

- [5] J. J. Rehr and R. C. Albers, Theoretical approaches to x-ray absorption fine structure, Rev. Mod. Phys. 72 (2000) 621.
- [6] P. Eisenberger and G. S. Brown, *X-ray absorption fine structure: Its applications and future*, Solid State Commun. **29** (1979) 481.
- [7] J. Emsley, *Nature's Building Blocks: An A-Z Guide to the Elements*. Oxford University Press, New York, 2 ed., 2011.
- [8] L. Wood, The Elements: Platinum. Cavendish Square Publishing LLC, New York, 2004.
- [9] M. Okube and A. Yoshiasa, Xafs measurement system for liquids at spring-8, J. Synchrotron Radiat. 8 (2001) 937.
- [10] N. B. Duc, V. Q. Tho, T. S. Tien, D. Q. Khoa and H. K. Hieu, Structure and optical properties of silver nanoparticles prepared by gamma co-60 irradiation, Radiat. Phys. Chem. 149 (2018) 61.
- [11] N. V. Hung, T. S. Tien, N. B. Duc and D. Q. Vuong, Local structure study of nanocrystalline ni-cu alloys by x-ray absorption fine structure spectroscopy, Mod. Phys. Lett. B 28 (2014) 1450174.
- [12] T. S. Tien, Local lattice distortion and charge density wave in laagsb2 probed by exafs, J. Phys. Soc. Jpn. 91 (2022) 054703.
- [13] T. Fujikawa and T. Miyanaga, *Ab initio multiple-scattering theory of x-ray-absorption fine structure and its applications*, J. Phys. Soc. Jpn. **62** (1993) 4108.
- [14] T. Yokoyama, K. Kobayashi, T. Ohta and A. Ugawa, X-ray-absorption fine-structure study of c<sub>60</sub> thin films, Phys. Rev. B 53 (1996) 6111.
- [15] N. V. Hung and J. J. Rehr, Ab initio calculations of x-ray absorption spectra of ni-based alloys, Phys. Rev. B 56 (1997) 43.
- [16] C. Kittel, Introduction to Solid State Physics. John Wiley & Sons, New York, 8 ed., 2004.
- [17] N. W. Ashcroft and N. D. Mermin, Solid State Physics. Holt-Rinehart & Winston, New York, 1976.
- [18] L. A. Girifalco and V. G. Weizer, Application of the mössbauer effect to studies of lattice dynamics, Phys. Rev. 114 (1959) 687.
- [19] E. Sevillano, H. Meuth and J. J. Rehr, *Normalized exafs: Improved accuracy and reliability of structural parameters*, Phys. Rev. B **20** (1979) 4908.
- [20] E. A. Stern, P. Livins and Z. Zhang, Multiple-scattering effects in x-ray-absorption fine structure, Phys. Rev. B 43 (1991) 8850.
- [21] I. V. Pirog, T. I. Nedoseikina, I. A. Zarubin and A. T. Shuvaev, *Xafs study of structural transformations in amorphous alloys*, J. Phys.: Condens. Matter **14** (2002) 1825.
- [22] I. V. Pirog and T. I. Nedoseikina, X-ray absorption fine structure study of amorphous metallic alloys, Physica B 334 (2003) 123.